

DualPrim: Compact 3D Reconstruction with Positive and Negative Primitives

Xiaoxu Meng^{1*}

xiaoxumeng.cs@gmail.com

Zhongmin Chen^{4,5*}

chenzhongmin19@mails.ucas.ac.cn

Bo Yang²

yangbo@waymo.com

Weikai Chen^{1†}

chenwk891@gmail.com

Weixiao Liu³

weixiaoliu@lucidmotors.com

Lin Gao^{4,5}

gaolin@ict.ac.cn

¹Independent Researcher ²Waymo LLC ³Lucid Motors

⁴Institute of Computing Technology, Chinese Academy of Sciences

⁵School of Advanced Interdisciplinary Science, University of Chinese Academy of Sciences

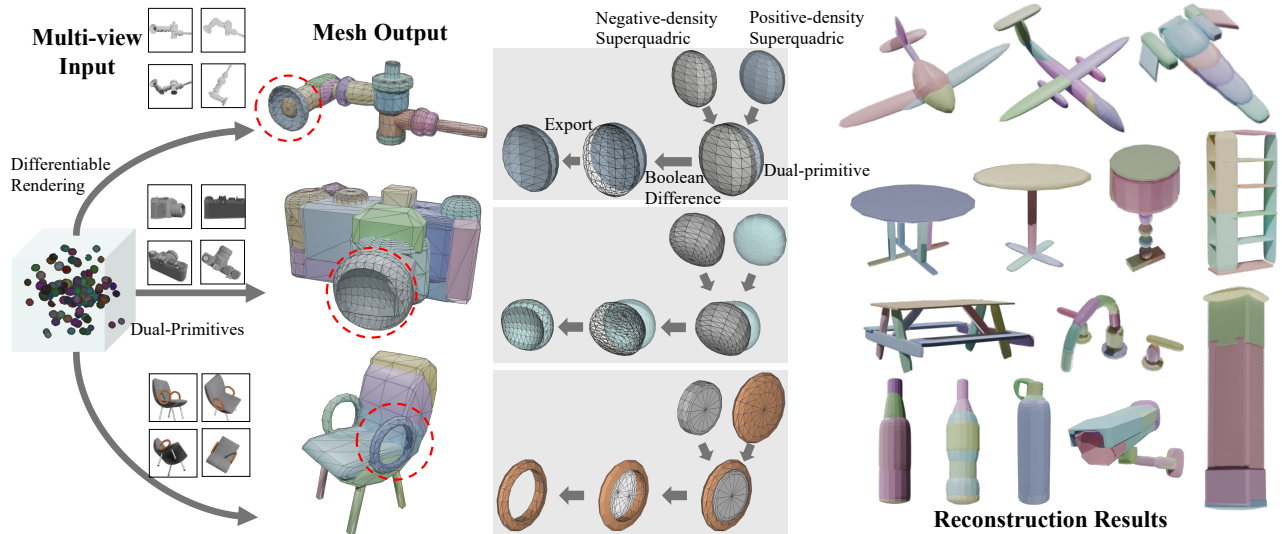


Figure 1. DualPrim is a differentiable representation that models 3D shapes using *dual-primitives* composed of positive- and negative-density superquadrics. This additive-subtractive design increases the representational power (e.g. holes and concavities) without sacrificing compactness or differentiability. Integrated into a volumetric differentiable renderer, DualPrim supports end-to-end learning from multi-view images and enables seamless mesh extraction through closed-form Boolean differencing. Our method produces compact, structured, and interpretable reconstructions that better meet downstream requirements than additive-only approaches.

Abstract

Neural reconstructions often trade structure for fidelity, yielding dense and unstructured meshes with irregular topology and weak part boundaries that hinder editing, animation, and downstream asset reuse. We present DualPrim, a compact and structured 3D reconstruction framework. Unlike additive-only implicit or primitive methods, DualPrim represents shapes with positive and negative superquadrics: the former builds the bases while the latter carves local volumes through a differentiable operator, en-

abling topology-aware modeling of holes and concavities. This additive-subtractive design increases the representational power without sacrificing compactness or differentiability. We embed DualPrim in a volumetric differentiable renderer, enabling end-to-end learning from multi-view images and seamless mesh export via closed-form boolean difference. Empirically, DualPrim delivers state-of-the-art accuracy and produces compact, structured, and interpretable outputs that better satisfy downstream needs than additive-only alternatives.

1. Introduction

Recent advances in neural reconstruction, such as NeRFs [32, 45, 59], SDFs [7, 54–56, 60], and Gaussian

*Equal contribution.

†Corresponding author, this paper solely reflects the author’s personal research and is not associated with the author’s affiliated institution.

Splatting (3DGS) [9, 13, 17, 21, 25, 57, 66], have achieved high-fidelity geometry modeling from multi-view images. However, these implicit or point-based representations produce dense and unstructured surfaces that are difficult to edit, animate, or integrate into standard graphics pipelines. Artists and designers, on the other hand, rely on *compact*, *structured*, and *part-based* meshes that explicitly capture both geometry and topology, as illustrated in Figure 2. The comparison highlights a key distinction: while artist-created meshes exhibit clean edge loops and consistent topology that support editing and animation [5, 49], meshes extracted from implicit fields via Marching Cubes [30] are typically over-tessellated and irregular, lacking meaningful part boundaries or structural organization. This contrast emphasizes a persistent gap between dense neural reconstructions and structured, interpretable geometry [31, 38, 39], motivating the need for representations that are compact, topologically regularized, and structurally meaningful.

Primitive-based reconstruction offers a promising step toward structured geometry by representing shapes as combinations of analytic primitives such as cuboids or superquadrics [40, 52]. Yet, most existing approaches rely solely on additive composition [40, 41, 52], accumulating positive volumetric fields to approximate target geometry. This additive nature inherently limits the ability to model topologically rich structures such as holes or concavities, which are ubiquitous in real-world objects [33].

Inspired by the constructive workflows used by 3D artists – where modeling involves both adding and carving volumes – We introduce DualPrim, a dual-primitive representation that pairs each positive superquadric with a negative one. The negative primitive acts as a differentiable carving operator, allowing the model to subtract local volumes and refine fine-scale structures while maintaining analytical regularity. This constructive-subtractive mechanism greatly expands the expressiveness of primitive-based representations without sacrificing compactness or differentiability. As shown in Figure 1, each dual-primitive is formed by combining a positive density superquadric that defines the constructive base shape with a negative density superquadric that carves out local regions through a differentiable boolean difference. This allows DualPrim to model a wide variety of geometries, from smooth convex shapes to intricate topologies with internal cavities or open parts, using only a compact set of analytic parameters.

To train such a representation, we formulate DualPrim within a differentiable rendering framework [38, 39] that jointly optimizes the parameters of positive and negative superquadrics from multi-view image supervision. Along each camera ray, we integrate the volumetric contributions of all primitives, combining additive and subtractive density fields in a continuous, differentiable manner. This unified formulation allows DualPrim to recover fine-

scale geometry directly from 2D observations, while naturally supporting mesh extraction through boolean difference operations [20]. Together, these design choices enable DualPrim to bridge the gap between dense neural reconstructions and structured 3D geometry. It produces meshes that are not only accurate and compact but also structurally organized, offering meaningful part decomposition and regular topology suitable for downstream applications such as editing, animation, simulation, and asset design [33].

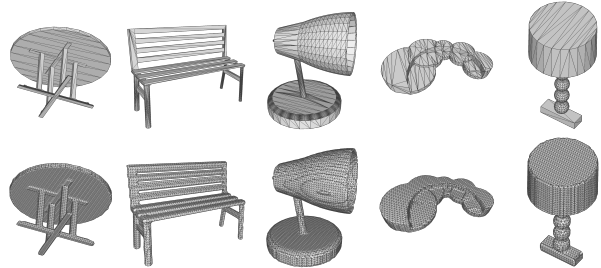


Figure 2. The first row shows the artist-created meshes (AMs), and the second row shows the exportation from Marching Cubes [30].

We evaluate on diverse multi-view reconstruction benchmarks covering a wide range of challenging 3D shapes. Our method consistently outperforms state-of-the-art approaches both qualitatively and quantitatively. Our main contributions can be summarized as:

- A new dual-primitive representation that pairs positive superquadrics with negative ones, enabling differentiable volume carving. This constructive-subtractive formulation improves topological expressiveness (holes, concavities) while preserving compactness and analyticity.
- A novel differentiable rendering framework that jointly learns additive and subtractive primitives from multi-view images in an end-to-end manner and supports direct mesh extraction via differentiable boolean operations.
- DualPrim establishes state-of-the-art reconstruction results with compact and structured geometry.

2. Related Work

Neural Implicit Reconstructions. Recent advances in 3D reconstruction leverage neural implicit and explicit representations to recover geometry from multi-view images [50]. NeRF-variants [32, 45, 59] optimize a continuous volumetric radiance field to produce high-fidelity novel views by fitting a per-scene neural field to input images. However, these methods do not provide explicit, compact surface representations, and rely on dense sampling and volumetric integration for geometry. SDF-based and hybrid SDF methods [7, 42, 54, 55, 60] including approaches that incorporate geometric priors for sparse-view reconstruction [35], and Tetrahedrons-based methods [36, 51] improve surface fidelity by representing geometry as learned SDFs or tetrahedral grids and adapting volume rendering to reduce geometric bias. Flexible isosurface extraction [47]

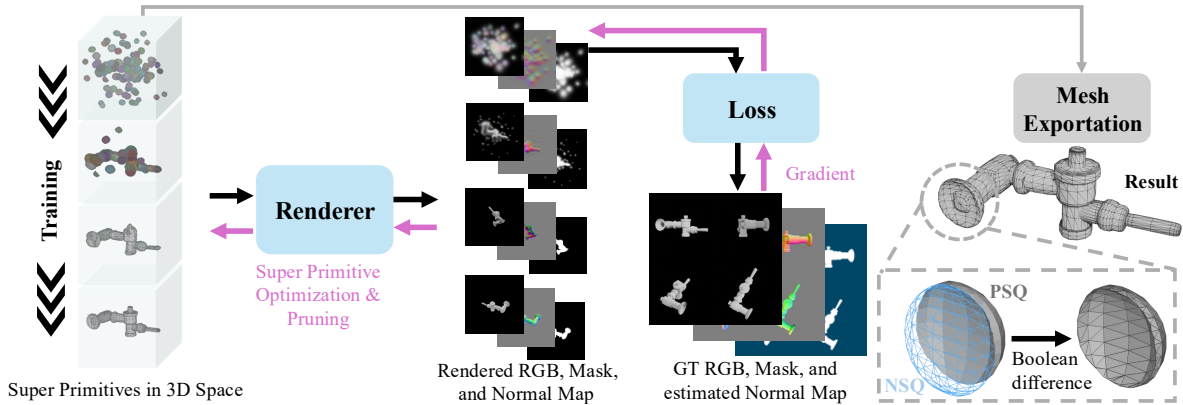


Figure 3. The overview of DualPrim pipeline. We represent the 3D scene as a set of primitive parameters and optimize them within a differentiable rendering framework under multi-view image supervision. The final mesh is obtained by computing the Boolean difference between the positive and negative superquadric components of each primitive.

further enables gradient-based mesh optimization by improving differentiability and geometric consistency during implicit-to-explicit conversion. While they achieve accurate zero-level surfaces, these methods inherit two key limitations: dependence on the implicit representation accuracy and sensitivity of subsequent mesh extraction to discretization and noise. Overall, these approaches produce photorealistic, dense surfaces, but their underlying representations are typically unstructured and lack part-level interpretability, limiting their applicability for tasks that require semantic understanding or structural manipulation. In contrast, explicit surface reconstruction methods generate watertight and feature-preserving meshes from 3D point clouds, such as optimal-transport-based mesh reconstruction for CAD models [63], but they are not differentiable and cannot be learned directly from image supervision.

Reconstruction from Model Retrieval and Constructive Methods. Alternatively, structured 3D shapes can be reconstructed via retrieval or alignment to pre-existing CAD models [2–4, 18, 19, 22, 53], though such approaches rely heavily on dataset priors. Constructive Solid Geometry (CSG) represents complex objects as hierarchical compositions of primitives via boolean operations. Neural CSG methods such as CSGNet [46], UCSG-Net [24], BSP-Net [12], CSG-Stump [44], CAPRI-Net [64] and D²CSG [65] learn to parse or generate symbolic CSG trees. However, neither model retrieval nor CSG-based approaches are differentiable, thereby hindering direct learning from images. Furthermore, hierarchical CSG parsing introduces combinatorial complexity: the search space of boolean trees grows exponentially with the number of primitives, which limits scalability to simple or low-part-count shapes. Earlier works explored learning shape composition from elementary primitives for interpretable 3D generation and matching [15], as well as convex decomposition to approximate shapes as unions of convex parts [14], improving fidelity while maintaining part interpretability, but its con-

vex parts are not explicitly aligned with semantic structure.

Superquadric Reconstruction via Differentiable Rendering. Superquadrics have a long history in geometric modeling [6, 43]. Recent works [16, 26–28, 58] revisit them for robust, differentiable shape abstraction. Methods such as Iterative Superquadric Recomposition [1] and Differentiable Blocks World [34] optimize primitive parameters from 2D images, while GaussianBlock [23] integrates Gaussian fields for editable decomposition. Neural Parts [41] learns implicit part-based representations that enable semantic consistency and part-level manipulation. However, it does not enforce explicit geometric primitives. Beyond image-based learning, EMS [27] and Marching-Primitives [28] extract structured superquadric representations directly from 3D data, offering compact and interpretable models. Most prior works, however, rely on additive composition and cannot capture holes or subtracted regions. PrimitiveAnything [62] extends this paradigm by formulating shape generation as an auto-regressive primitive assembly task. DualVector [29] leverages Boolean operations to produce editable vector representations, but it is restricted to 2D and lacks explicit primitive-based geometric regularization. Our approach addresses this by incorporating both positive and negative superquadrics, enabling differentiable modeling of additive and subtractive relationships for expressive shape abstraction.

Artist-Created Mesh Generation. Complementary to reconstruction, recent generative works aim to mimic artist-created mesh design. MeshGPT [48] and PolyGen [37] generate meshes autoregressively from a learned geometric vocabulary, while MeshAnything [10, 11] converts 3D assets into artist-style meshes using transformer-based architectures. Our approach differs in that it performs part-aware reconstruction directly from multi-view images rather than unconditional mesh generation, combining interpretability with geometric fidelity.

3. Method

We propose a super-primitive based rendering framework that integrates both positive and negative shape components for compact 3D representation. The overall pipeline of our method is illustrated in Figure 3. For each pixel on an input image, we sample N points along the camera ray $\{\mathbf{p}(t_i) = \mathbf{o} + t_i\mathbf{v} \mid i = 1, 2, \dots, N\}$, where \mathbf{o} denotes the camera center and \mathbf{v} is the corresponding view direction. We implicitly represent the surface as a signed distance field (SDF) $f(\mathbf{p}(t_i)) : \mathbb{R}^3 \rightarrow \mathbb{R}$. By accumulating the SDF-based densities σ and colors \mathbf{c}_i of the sampled points, the predicted image I_{render} is computed as:

$$I_{render}(\mathbf{o}, \mathbf{v}) = \sum_{i=1}^N \left(\prod_{j=1}^{i-1} (1 - \alpha_j) \right) \alpha_i \mathbf{c}_i, \quad (1)$$

where $\alpha_i = 1 - \exp(-\sigma_i \delta_i)$. Here, $\delta_i = t_{i+1} - t_i$ is the distance between adjacent samples. To render a full image, we just need to calculate the SDF and the auxiliary features from the dual-primitive-based geometric representation.

3.1. Formulation

We represent each dual-primitive with two superquadrics defined by the implicit equation:

$$f(x, y, z) = \left(\left(\frac{x}{a_x} \right)^{\frac{2}{\epsilon_2}} + \left(\frac{y}{a_y} \right)^{\frac{2}{\epsilon_2}} \right)^{\frac{\epsilon_2}{\epsilon_1}} + \left(\frac{z}{a_z} \right)^{\frac{2}{\epsilon_1}} \frac{\epsilon_1}{2} = 1.$$

The first superquadric serves as a positive shape generator, referred to as the ‘‘positive density superquadric’’ (PSQ), while the second acts as a subtractive component, referred to as the ‘‘negative density superquadric’’ (NSQ). As shown in Figure 1, the NSQ functions like an eraser; it is effective only when overlapping with the PSQ, where it removes density within the intersection region. If there is no overlap, the NSQ has zero contribution to the mesh, and the dual-primitive degenerates into one PSQ only. This design significantly expands the representational capacity, enabling asymmetric and complex shapes beyond the limitations of conventional superquadrics.

Since the wireframe of each superquadric can be represented as edge loops, we can extract the 3D mesh of a dual-primitive by computing the Boolean difference between the meshes of its PSQ and NSQ components. To learn dual-primitives directly from 2D observations, we parameterize each primitive as summarized in Table 1, and define a differentiable rendering process based on these parameters.

3.2. Renderer

Based on Equation 1, the central challenge in rendering is estimating an appropriate density field σ . To achieve this, we first estimate the implicit surface function (ISF) for each point under every primitive, and then derive the corresponding probability density function from the ISF and primitive parameters of the K dual-primitives.

Implicit Surface Estimation. For each dual-primitive S , the implicit surface function $f(\mathbf{p}, Q)$ for each superquadric Q (either PSQ or NSQ) for each 3D point \mathbf{p} is defined as:

$$f(\mathbf{p}, Q) = \left(\left(\frac{\mathbf{p}'_x}{a_{x,Q}} \right)^{\frac{2}{\epsilon_{2,Q}}} + \left(\frac{\mathbf{p}'_y}{a_{y,Q}} \right)^{\frac{2}{\epsilon_{2,Q}}} \right)^{\frac{\epsilon_{2,Q}}{\epsilon_{1,Q}}} + \left(\frac{\mathbf{p}'_z}{a_{z,Q}} \right)^{\frac{2}{\epsilon_{1,Q}}} \frac{\epsilon_{1,Q}}{2} - 1, \quad (2)$$

where \mathbf{p}' denotes the 3D coordinate in the local frame of the superquadric, obtained by:

$$\mathbf{p}' = R_Q^{-1}(\mathbf{p} - T_Q). \quad (3)$$

After obtaining the ISF for PSQ and NSQ, we compute the ISF of the combined dual-primitive by subtracting the contribution of the NSQ from the PSQ.

To conduct the subtraction, we estimate P_E , the probability that the NSQ is effective, as:

$$P_E(\mathbf{p}, S) = \Phi\left(-\frac{f(\mathbf{p}, PSQ)}{\theta_S(\mathbf{p})} - \mu\right) \cdot \Phi\left(-\frac{f(\mathbf{p}, NSQ)}{\theta_S(\mathbf{p})} - \mu\right), \quad (4)$$

where $\Phi(x) = (1 + \exp(-x))^{-1}$ is the Sigmoid function, and μ is a small offset ensuring that zero-crossings are preserved. P_E attains high values only when \mathbf{p} lies within both PSQ and NSQ and the primitive is sufficiently sharp. The merged ISF $f(\mathbf{p}, S)$ and normal $\mathbf{n}(\mathbf{p}, S)$ are computed as:

$$f(\mathbf{p}, S) = f(\mathbf{p}, PSQ) \cdot (1 - P_E(\mathbf{p}, S)) - f(\mathbf{p}, NSQ) \cdot P_E(\mathbf{p}, S), \quad (5)$$

$$\mathbf{n}(\mathbf{p}, S) = \mathbf{Normalize}(f'(\mathbf{p}, PSQ)) \cdot (1 - P_E(\mathbf{p}, S)) - \mathbf{Normalize}(f'(\mathbf{p}, NSQ)) \cdot P_E(\mathbf{p}, S). \quad (6)$$

We provide a 2D illustration of this subtraction mechanism in Figure 4. The ray-surface intersections and the resulting ISF transitions demonstrate how NSQ effectively erases portions of PSQ, creating complex composite shapes through a simple probabilistic formulation.

Probability Density Estimation. Following NeuS [54], we estimate the volume density of each primitive from the ISF values as:

$$\sigma_S(\mathbf{p}) = \max\left(\frac{\Phi\left(\frac{f(\mathbf{p}+\Delta\mathbf{p}, S)}{\theta_S}\right) - \Phi\left(\frac{f(\mathbf{p}-\Delta\mathbf{p}, S)}{\theta_S}\right)}{\Phi\left(\frac{f(\mathbf{p}+\Delta\mathbf{p}, S)}{\theta_S}\right)}, 0\right). \quad (7)$$

The final point-wise density is then obtained by summing over all K dual-primitives: $\sigma(\mathbf{p}) = \sum_{k=1}^K \alpha_{S_k}(\mathbf{p}) \cdot \sigma_{S_k}(\mathbf{p})$. We consider that the color of the point is affected by the texture and the lighting condition. We use Equation 8 to calculate the color of the point. Here, $C(\mathbf{p}) \in \mathbb{R}^3$ is the texture and lighting predicted with an MLP.

Parameter Name	Shape	Explanation	Range
scale parameters (a_x, a_y, a_z)	(2, 3)	The radius of the x-, y-, z-axis of PSQ and NSQ.	[0.02, 1.0]
shape parameters (ϵ_1, ϵ_2)	(2, 2)	The parameters controlling the shape of PSQ and NSQ.	[0.05, 2]
primitive transparency α	(1)	The transparency of the super-primitive.	[0, 1]
primitive render sharpness θ	(1)	The sharpness of the super-primitive.	[0, 1]
translation T	(2, 3)	The translation of the PSQ and the NSQ.	[-1, 1]
rotation R	(2, 3)	The rotation angles of the PSQ and the NSQ.	[-180, 180]
basic color c_{basic}	(3)	The basic RGB color of the super-primitive.	[0, 1]

Table 1. The full parameter list of a super primitive.

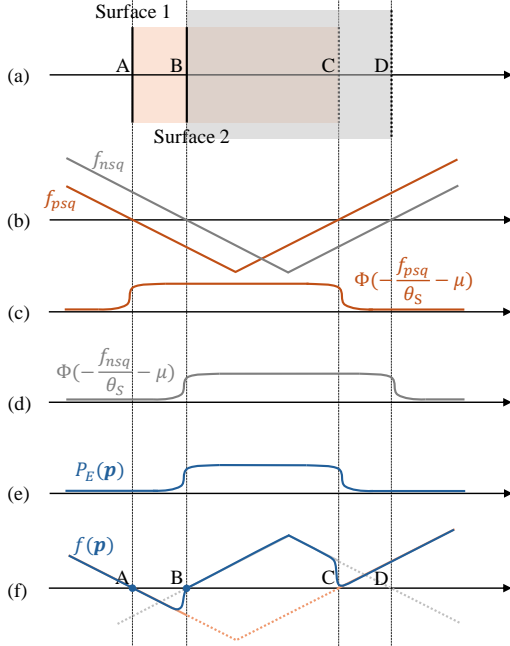


Figure 4. Illustration of the SDF calculation with PSQ and NSQ.

$$\mathbf{c}(\mathbf{p}) = \sum_k c_{basic}(\mathbf{p}, S_k) \cdot \frac{\sigma_{S_k}(\mathbf{p})}{\sigma(\mathbf{p})} + C(\mathbf{p}), \quad (8)$$

Similarly, we render the mask $M_{render}(\mathbf{o}, \mathbf{v})$ and normal map $N_{render}(\mathbf{o}, \mathbf{v})$ using volume accumulation:

$$M_{render}(\mathbf{o}, \mathbf{v}) = \sum_{i=1}^N \left(\prod_{j=1}^{i-1} (1 - \alpha_j) \right) \alpha_i. \quad (9)$$

$$N_{render}(\mathbf{o}, \mathbf{v}) = \sum_{i=1}^N \left(\prod_{j=1}^{i-1} (1 - \alpha_j) \right) \alpha_i \mathbf{n}_i, \quad (10)$$

where each \mathbf{n}_i is computed as:

$$\mathbf{n}(\mathbf{p}) = \sum_k \mathbf{n}_{p, S_k}(\mathbf{p}, S_k) \cdot \frac{\sigma_{S_k}(\mathbf{p})}{\sigma(\mathbf{p})}. \quad (11)$$

As demonstrated in Figure 5, our renderer effectively synthesizes diverse primitives with controllable shape, color, transparency, and surface sharpness, enabling accurate 3D reconstruction and fine-grained structure representation.

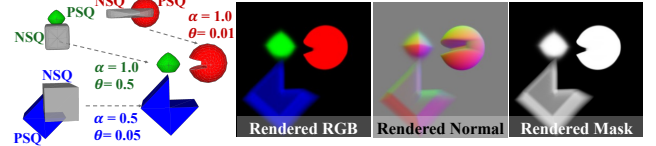


Figure 5. We show the rendering of three example dual-primitives.

3.3. Mesh Exportation

In the mesh extraction stage, we discard primitives with low transparency ($\alpha < T_{export} = 0.5$) and export the meshes corresponding to both PSQs and NSQs. The final object mesh is obtained by performing a Boolean difference operation between the PSQ and NSQ meshes, allowing precise geometric reconstruction of complex structures and maintaining structured and regularized wireframes.

4. Optimization

4.1. Training Objectives

We supervise the training of DualPrim-Net using six loss terms, formulated as:

$$\begin{aligned} \mathcal{L} = & \mathcal{L}_{rgb} + \lambda_{mask} \cdot \mathcal{L}_{mask} + \lambda_{sparse} \cdot \mathcal{L}_{sp} + \lambda_e \cdot \mathcal{L}_e \\ & + \lambda_{max} \cdot \mathcal{L}_{max} + \lambda_{norm_reg} \cdot \mathcal{L}_{norm_reg}. \end{aligned} \quad (12)$$

The overall objective combines photometric, geometric, and structural regularizations to ensure faithful reconstruction and stable optimization. The first two terms correspond to photometric and mask supervision, respectively:

$$\mathcal{L}_{rgb} = \sum_{i,j} \|I_{render}(i,j) - I_{gt}(i,j)\| \cdot M_{gt}(i,j), \quad (13)$$

$$\mathcal{L}_{mask} = \sum_{i,j} BCE(M_{render}(i,j), M_{gt}(i,j)). \quad (14)$$

Beyond direct supervision, we use 4 regularization terms to enhance structural compactness and geometric consistency.

Redundant Suppression. To discourage using redundant dual-primitives and promote compact surface, we impose a sparsity loss that penalizes excessive opacity:

$$\mathcal{L}_{sp} = \frac{1}{K} \sum_{\mathbf{p}} \alpha(\mathbf{p}). \quad (15)$$

Rendering Probability Entropy Regularization. Since an object’s physical presence is inherently binary (either exists or not), the transparency $\alpha(\mathbf{p})$ should ideally converge to 0 or 1. To encourage such deterministic behavior, we minimize the entropy of $\alpha(\mathbf{p})$:

$$\mathcal{L}_e = -\frac{1}{K} \sum_{\mathbf{p}} \alpha(\mathbf{p}) \log(\alpha(\mathbf{p})) + (1 - \alpha(\mathbf{p})) \log((1 - \alpha(\mathbf{p}))). \quad (16)$$

Rendering Probability Maximum Value Regularization. Physically, the surface existence probability should not exceed 1. To enforce this constraint, we introduce a max-value regularization that softly penalizes $\alpha(\mathbf{p}) > 1$:

$$\mathcal{L}_{max} = \frac{1}{K} \sum_{\mathbf{p}} \text{ReLU}(\alpha(\mathbf{p}) - 1). \quad (17)$$

Normal Consistency Regularization. To further encourage geometrically coherent reconstruction, we add a normal consistency term. This loss enforces agreement between the predicted surface normal $N_{render}(i, j)$ and a reference normal $N_{Pred}(i, j)$, which is estimated directly from the rendered surface without requiring additional annotations:

$$\mathcal{L}_{norm.reg} = \sum_{i,j} \|N_{render}(i, j) - N_{Pred}(i, j)\| \cdot M_{gt}(i, j). \quad (18)$$

Together, these loss terms jointly guide the model to produce compact, physically plausible, and geometrically consistent reconstructions.

4.2. Adaptive Control of Dual-primitives

We initialize the reconstruction with a dense set of randomly distributed dual-primitives and progressively refine this set through adaptive pruning. This adaptive process iteratively removes redundant primitives and retains only those essential to accurately represent the target structure.

Pruning Strategy. Following a strategy similar to 3DGS [25], we use the primitive transparency parameter α as a key pruning criterion. Specifically, dual-primitives with $\alpha < 0.02$ are discarded, as they contribute negligibly to the final rendering. To avoid numerical instability and preserve structural clarity, we also remove primitives whose scale parameters fall below a threshold $t_a = 0.01$. This ensures that all retained primitives correspond to meaningful, spatially significant parts of the object.

View-dependent Filtering. We prune primitives with negligible rendering weights across all viewpoints — typically those fully occluded or visually redundant. This pruning is performed periodically during training, allowing the model to dynamically reallocate representational capacity toward visible and structurally informative regions.

Through this adaptive control mechanism, the model evolves from a dense initialization to a compact, interpretable, and efficient primitive representation, leading to faster convergence and improved reconstruction quality.

5. Experiments

5.1. Experimental Setup

Datasets. We evaluate DualPrim on multi-view reconstruction tasks to demonstrate its ability to achieve state-of-the-art reconstruction quality while maintaining a compact and regularized wireframe representation. Experiments are conducted on 12 categories from the ShapeNet dataset [8], with 15 objects randomly sampled per category to cover a diverse range of textures and geometries. We uniformly sample 24 viewpoints on the unit sphere, adding top and bottom views to obtain 26 camera positions. Ground truth 3D models are rendered using *Blender* at a resolution of 256×256 . All experiments are evaluated against representative state-of-the-art methods.

Implementation details. We initialize $K = 100$ dual-primitives randomly in the $[-1, 1]$ space. The MLP for lighting consists of 4 layers with Xavier initialization.

Baselines. We compare DualPrim with state-of-the-art methods across 5 categories: volume rendering-based method RNb-NeuS (RNS) [7], Gaussian-based method 2DGS [21], tetrahedron-based method nvdifrec (NVD) [36], shape abstraction methods EMS [27], Marching Primitives (MP) [28], PrimitiveAnything (PA) [62], CapriNet (CAPRI) [64], D²CSG [65], DiffCSG [67], and topology optimization methods Flexicubes (FC) [47] and MeshAnything (MA) [10].

For PA, MA, MP, EMS, NVD, FC, CAPRI, D²CSG, and DiffCSG, SDF values exported from RNb-NeuS are used as the input. For 2DGS+MC and 2DGS+CSG, we use the SDF exported from 2DGS as the input. Normal maps estimated by StableNormal [61] are employed as supervision for both our method and RNb-NeuS.

5.2. Reconstruction from Multi-view Images

We report Chamfer Distance (CD) averaged over 180 examples in Table 2. DualPrim achieves lower reconstruction errors compared to state-of-the-art approaches. RNb-NeuS [7], 2DGS [21] and nvdifrec [36], which extract 3D meshes from SDF grids using Marching Cubes [30] or Marching Tetrahedrons [51], tend to produce over-tessellated surfaces with limited geometric regularity. Flexicubes [47] recovers structured geometry, but grid-based mesh extraction can degrade fine details relative to meshes generated from primitives. Primitive-based methods, including Marching Primitives [28], CapriNet [64], D²CSG [65], DiffCSG [67], EMS [27], Me-



Figure 6. Qualitative comparison on in-the-wild objects. Each object occupies two rows. The first row shows input, Ours, PA, MA, MP, EMS, and NVD. The second row shows FC, RNS, CAPRI, D^2 CSG, DiffCSG, 2DGS+MC, and 2DGS+CSG.

shAnything [10], and PrimitiveAnything [62], achieve compact and interpretable meshes; however, the reconstruction quality depends on the underlying SDF and can be affected by noise and data loss.

We show qualitative results in Figure 6. While most

methods successfully reconstruct the overall geometry, their outputs exhibit varying levels of fidelity and compactness. RNb-NeuS [7], 2DGS [21] and nvdifrec [36], which extract 3D meshes from SDF grids using Marching Cubes [30] or Marching Tetrahedrons [51], tend to produce overly tessel-

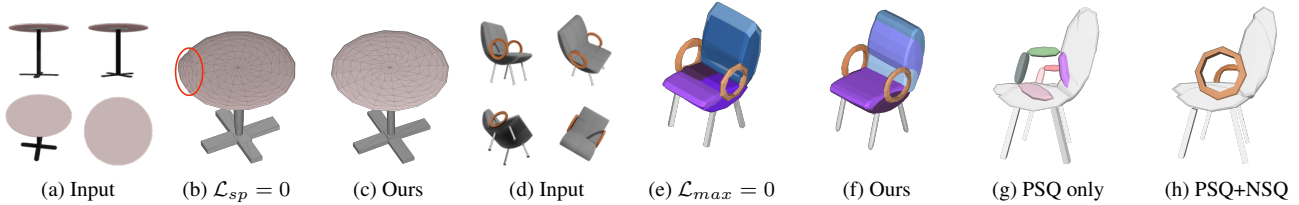


Figure 7. The ablation study on regularization terms.

lated surfaces that fail to respect underlying geometric regularities. Flexicubes [47] demonstrates an ability to recover structured geometry; however, its reliance on grid-based mesh extraction can further degrade fine details compared to meshes directly generated via Marching Cubes. Methods such as MP [28], MA [10], PA [62], CAPRI [64], D²CSG [65], DiffCSG [67] improve mesh compactness, but their reconstruction quality remains highly sensitive to the imperfections of the underlying SDF, which often manifest as surface artifacts and redundancies in the reconstructed meshes. In contrast, DualPrim reconstructs compact, high-fidelity meshes that closely preserve the shape and topological characteristics of artist-designed models. Additional qualitative and per-category quantitative results are provided in the supplementary material.

5.3. User Study on Geometry Editability

We conducted a user study to evaluate geometric editability compared to baselines. Twelve representative cases were randomly selected, and 36 participants with 3D mesh editing experience rated editability and structural controllability scored from 1 to 10. The results, summarized in second row of Table 2, show that DualPrim produces compact and structured geometric representations with significantly higher editability scores compared to prior methods. Further details are provided in the supplementary material.

Method	#V(k)↓	#F(k)↓	NC Loss↓	CD↓	EditScore↑
RNS [7]	124.41	57.44	37.45	10.71	4.77
NVD [36]	15.40	13.98	56.19	10.63	5.47
FC [47]	16.67	8.33	16.11	13.32	4.98
PA [62]	21.51	12.61	4.48	11.57	4.59
MP [28]	3.38	1.75	12.42	12.58	4.88
MA [10]	0.55	0.29	4.00	10.12	5.12
EMS [27]	2.40	1.22	9.02	16.64	3.92
2DGS [21] + MC	151.71	75.95	53.75	12.06	3.75
2DGS [21] + CSG	44.83	18.10	16.66	12.63	4.41
DiffCSG [67]	10.24	5.20	8.20	11.27	5.50
CAPRI [64]	29.07	12.64	11.55	11.28	4.98
D ² CSG [65]	24.27	11.62	13.21	12.12	4.73
Ours	1.54	0.79	7.73	7.94	8.29

Table 2. Quantitative comparison and user evaluation of DualPrim (ours) with 13 representative methods.

5.4. Ablation Study

Ablation on regularization. Comparing Figures 7 (b) and (c), we observe that setting $\mathcal{L}_{sp} = 0$ results in redundant primitives, rather than encouraging the model to use a

sparse set. Similarly, comparing Figures 7 (e) and (f), setting $\mathcal{L}_{max} = 0$ leads to multiple primitives with overlaps, instead of representing the geometry with a single primitive.

Ablation on PSQ-only training. Figure 7 (g) and (h) compares the reconstruction using only PSQ versus using both PSQ and NSQ. Incorporating NSQ allows the model to subtract local volumes and refine fine-scale structures while maintaining analytical regularity.

6. Conclusion and Future Work

We introduce DualPrim, a novel algorithm for reconstructing artist-style 3D meshes from multi-view images. Our approach employs a primitive-based representation that is both compact and differentiable, enabling seamless integration with volume rendering pipelines. Extensive experiments demonstrate that DualPrim outperforms current state-of-the-art methods in reconstruction accuracy, compactness, and topological quality across diverse object categories. We believe this advancement will have a significant impact on the generation of 3D assets for gaming and the metaverse, and has the potential to inspire further research in areas such as physics simulation and collision detection. Nevertheless, our algorithm has certain limitations. It struggles to accurately capture object parts that are thinner than the voxel grid resolution, though this can be mitigated by increasing the grid resolution or thickening the affected regions. Another limitation is primitive overlap. Although the regularization terms substantially reduce overlap, minor edge-level or layout-induced intersections may still occur. These small overlaps do not noticeably affect reconstruction fidelity or downstream editability. Furthermore, the method is primarily tailored for industrially designed objects with well-defined structures and demonstrates reduced performance on real-world objects with irregular or less structured geometries.

Acknowledgements. This work was supported by the National Natural Science Foundation of China (No. 62322210, 62561160115). We would like to thank the anonymous reviewers for their constructive feedback and insightful suggestions, which helped improve the quality of this work. We also thank Haocheng Yuan and Yixuan Li for their generous assistance in running the comparison experiments for DiffCSG and PrimitiveAnything.

References

- [1] Stephan Alaniz, Massimiliano Mancini, and Zeynep Akata. Iterative superquadric recomposition of 3d objects from multiple views. In *Proceedings of the IEEE/CVF International Conference on Computer Vision*, pages 18013–18023, 2023. 3
- [2] Armen Avetisyan, Manuel Dahnert, Angela Dai, Manolis Savva, Angel X. Chang, and Matthias Nießner. Scan2cad: Learning cad model alignment in rgb-d scans. In *2019 IEEE/CVF Conference on Computer Vision and Pattern Recognition (CVPR)*, pages 2609–2618, 2019. 3
- [3] Armen Avetisyan, Angela Dai, and Matthias Niessner. End-to-end cad model retrieval and 9dof alignment in 3d scans. In *2019 IEEE/CVF International Conference on Computer Vision (ICCV)*, pages 2551–2560, 2019.
- [4] Armen Avetisyan, Tatiana Khanova, Christopher Choy, Denver Dash, Angela Dai, and Matthias Nießner. Scenecad: Predicting object alignments and layouts in rgb-d scans. In *The European Conference on Computer Vision (ECCV)*, 2020. 3
- [5] Ilya Baran and Jovan Popović. Automatic rigging and animation of 3d characters. *ACM Transactions on graphics (TOG)*, 26(3):72–es, 2007. 2
- [6] Alan H Barr. Superquadrics and angle-preserving transformations. *IEEE Computer graphics and Applications*, 1(01): 11–23, 1981. 3
- [7] Baptiste Brument, Robin Bruneau, Yvain Quéau, Jean Mérou, François Lauze, Jean-Denis Durou, and Lilian Calvet. Rnb-neus: Reflectance and normal-based multi-view 3d reconstruction. In *IEEE/CVF Conference on Computer Vision and Pattern Recognition (CVPR)*, 2024. 1, 2, 6, 7, 8
- [8] Angel X. Chang, Thomas Funkhouser, Leonidas Guibas, Pat Hanrahan, Qixing Huang, Zimo Li, Silvio Savarese, Manolis Savva, Shuran Song, Hao Su, Jianxiong Xiao, Li Yi, and Fisher Yu. ShapeNet: An Information-Rich 3D Model Repository. Technical Report arXiv:1512.03012 [cs.GR], Stanford University — Princeton University — Toyota Technological Institute at Chicago, 2015. 6
- [9] Guikun Chen and Wenguan Wang. A survey on 3d gaussian splatting. *arXiv preprint arXiv:2401.03890*, 2024. 2
- [10] Yiwen Chen, Tong He, Di Huang, Weicai Ye, Sijin Chen, Jiayang Tang, Xin Chen, Zhongang Cai, Lei Yang, Gang Yu, Guosheng Lin, and Chi Zhang. Meshanything: Artist-created mesh generation with autoregressive transformers, 2024. 3, 6, 7, 8
- [11] Yiwen Chen, Yikai Wang, Yihao Luo, Zhengyi Wang, Zilong Chen, Jun Zhu, Chi Zhang, and Guosheng Lin. Meshanything v2: Artist-created mesh generation with adjacent mesh tokenization, 2024. 3
- [12] Zhiqin Chen, Andrea Tagliasacchi, and Hao Zhang. Bspnet: Generating compact meshes via binary space partitioning. *Proceedings of IEEE Conference on Computer Vision and Pattern Recognition (CVPR)*, 2020. 3
- [13] Zilong Chen, Feng Wang, Yikai Wang, and Huaping Liu. Text-to-3d using gaussian splatting. In *Proceedings of the IEEE/CVF Conference on Computer Vision and Pattern Recognition (CVPR)*, pages 21401–21412, 2024. 2
- [14] Boyang Deng, Kyle Genova, Soroosh Yazdani, Sofien Bouaziz, Geoffrey Hinton, and Andrea Tagliasacchi. Cvxnet: Learnable convex decomposition. 2020. 3
- [15] Theo Deprelle, Thibault Groueix, Matthew Fisher, Vladimir Kim, Bryan Russell, and Mathieu Aubry. Learning elementary structures for 3d shape generation and matching. *Advances in Neural Information Processing Systems*, 32, 2019. 3
- [16] Elisabetta Fedele, Boyang Sun, Leonidas Guibas, Marc Pollefeys, and Francis Engelmann. SuperDec: 3D Scene Decomposition with Superquadric Primitives. In *Proceedings of the IEEE/CVF International Conference on Computer Vision (ICCV)*, 2025. 3
- [17] Ben Fei, Jingyi Xu, Rui Zhang, Qingyuan Zhou, Weidong Yang, and Ying He. 3d gaussian as a new vision era: A survey. *arXiv preprint arXiv:2402.07181*, 2024. 2
- [18] Daoyi Gao, David Rozenberszki, Stefan Leutenegger, and Angela Dai. Diffcad: Weakly-supervised probabilistic cad model retrieval and alignment from an rgb image. *ACM Trans. Graph.*, 43(4), 2024. 3
- [19] Can Gümeli, Angela Dai, and Matthias Nießner. Roca: Robust cad model retrieval and alignment from a single image. In *Proceedings of the IEEE/CVF Conference on Computer Vision and Pattern Recognition (CVPR)*, pages 4022–4031, 2022. 3
- [20] Amir Hertz, Or Perel, Raja Giryes, Olga Sorkine-Hornung, and Daniel Cohen-Or. Spaghetti: Editing implicit shapes through part aware generation. *ACM Transactions on Graphics (TOG)*, 41(4):1–20, 2022. 2
- [21] Binbin Huang, Zehao Yu, Anpei Chen, Andreas Geiger, and Shenghua Gao. 2d gaussian splatting for geometrically accurate radiance fields. In *ACM SIGGRAPH 2024 Conference Papers*, pages 1–11, 2024. 2, 6, 7, 8
- [22] Vladislav Ishimtsev, Alexey Bokhovkin, Alexey Artemov, Savva Ignatyev, Matthias Niessner, Denis Zorin, and Evgeny Burnaev. Cad-deform: Deformable fitting of cad models to 3d scans. In *Computer Vision – ECCV 2020*, pages 599–628, Cham, 2020. Springer International Publishing. 3
- [23] Shuyi Jiang, Qihao Zhao, Hossein Rahmani, De Wen Soh, Jun Liu, and Na Zhao. Gaussianblock: Building part-aware compositional and editable 3d scene by primitives and gaussians. *arXiv preprint arXiv:2410.01535*, 2024. 3
- [24] Kacper Kania, Maciej Zieba, and Tomasz Kajdanowicz. Ucsq-net-unsupervised discovering of constructive solid geometry tree. *Advances in neural information processing systems*, 33:8776–8786, 2020. 3
- [25] Bernhard Kerbl, Georgios Kopanas, Thomas Leimkühler, and George Drettakis. 3d gaussian splatting for real-time radiance field rendering. *ACM Trans. Graph.*, 42(4):139–1, 2023. 2, 6
- [26] Young Hun Kim, Seungyeon Kim, Yonghyeon Lee, and Frank C. Park. T²SQNet: A recognition model for manipulating partially observed transparent tableware objects. In *8th Annual Conference on Robot Learning*, 2024. 3
- [27] Weixiao Liu, Yuwei Wu, Sipu Ruan, and Gregory S. Chirikjian. Robust and Accurate Superquadric Recovery: a Probabilistic Approach. In *2022 IEEE/CVF Conference*

- on *Computer Vision and Pattern Recognition (CVPR)*, pages 2666–2675, Los Alamitos, CA, USA, 2022. IEEE Computer Society. 3, 6, 7, 8
- [28] Weixiao Liu, Yuwei Wu, Sipu Ruan, and Gregory Chirikjian. Marching-primitives: Shape abstraction from signed distance function. In *Proceedings IEEE Conf. on Computer Vision and Pattern Recognition (CVPR)*, 2023. 3, 6, 7, 8
- [29] Ying-Tian Liu, Zhifei Zhang, Yuan-Chen Guo, Matthew Fisher, Zhaowen Wang, and Song-Hai Zhang. Dualvector: Unsupervised vector font synthesis with dual-part representation. In *Proceedings of the IEEE/CVF Conference on Computer Vision and Pattern Recognition (CVPR)*, pages 14193–14202, 2023. 3
- [30] William E. Lorensen and Harvey E. Cline. Marching cubes: A high resolution 3d surface construction algorithm. In *Proceedings of the 14th Annual Conference on Computer Graphics and Interactive Techniques*, page 163–169, New York, NY, USA, 1987. Association for Computing Machinery. 2, 6, 7
- [31] Lars Mescheder, Michael Oechsle, Michael Niemeyer, Sebastian Nowozin, and Andreas Geiger. Occupancy networks: Learning 3d reconstruction in function space. In *Proceedings of the IEEE/CVF conference on computer vision and pattern recognition*, pages 4460–4470, 2019. 2
- [32] Ben Mildenhall, Pratul P Srinivasan, Matthew Tancik, Jonathan T Barron, Ravi Ramamoorthi, and Ren Ng. Nerf: Representing scenes as neural radiance fields for view synthesis. In *European conference on computer vision*, pages 405–421. Springer, 2020. 1, 2
- [33] Kaichun Mo, Paul Guerrero, Li Yi, Hao Su, Peter Wonka, Niloy J Mitra, and Leonidas J Guibas. Structedit: Learning structural shape variations. In *Proceedings of the IEEE/CVF Conference on Computer Vision and Pattern Recognition*, pages 8859–8868, 2020. 2
- [34] Tom Monnier, Jake Austin, Angjoo Kanazawa, Alexei Efros, and Mathieu Aubry. Differentiable blocks world: Qualitative 3d decomposition by rendering primitives. *Advances in Neural Information Processing Systems*, 36:5791–5807, 2023. 3
- [35] Tai-Jiang Mu, Hao-Xiang Chen, Jun-Xiong Cai, and Ning Guo. Neural 3d reconstruction from sparse views using geometric priors. *Computational Visual Media*, 9(4):687–697, 2023. 2
- [36] Jacob Munkberg, Jon Hasselgren, Tianchang Shen, Jun Gao, Wenzheng Chen, Alex Evans, Thomas Müller, and Sanja Fidler. Extracting Triangular 3D Models, Materials, and Lighting From Images. In *Proceedings of the IEEE/CVF Conference on Computer Vision and Pattern Recognition (CVPR)*, pages 8280–8290, 2022. 2, 6, 7, 8
- [37] Charlie Nash, Yaroslav Ganin, SM Ali Eslami, and Peter Battaglia. Polygen: An autoregressive generative model of 3d meshes. In *International conference on machine learning*, pages 7220–7229. PMLR, 2020. 3
- [38] Michael Niemeyer, Lars Mescheder, Michael Oechsle, and Andreas Geiger. Differentiable volumetric rendering: Learning implicit 3d representations without 3d supervision. In *Proceedings of the IEEE/CVF Conference on Computer Vision and Pattern Recognition*, pages 3504–3515, 2020. 2
- [39] Michael Oechsle, Songyou Peng, and Andreas Geiger. Unisurf: Unifying neural implicit surfaces and radiance fields for multi-view reconstruction. In *Proceedings of the IEEE/CVF International Conference on Computer Vision*, pages 5589–5599, 2021. 2
- [40] Despoina Paschalidou, Ali Osman Ulusoy, and Andreas Geiger. Superquadrics revisited: Learning 3d shape parsing beyond cuboids. In *Proceedings of the IEEE/CVF conference on computer vision and pattern recognition*, pages 10344–10353, 2019. 2
- [41] Despoina Paschalidou, Angelos Katharopoulos, Andreas Geiger, and Sanja Fidler. Neural parts: Learning expressive 3d shape abstractions with invertible neural networks. In *Proceedings of the IEEE/CVF Conference on Computer Vision and Pattern Recognition*, pages 3204–3215, 2021. 2, 3
- [42] Zhexi Peng, Kun Zhou, and Tianjia Shao. Gaussian-plus-sdf slam: High-fidelity 3d reconstruction at 150+ fps. *Computational Visual Media*, 2025. 2
- [43] Alex P Pentland. Perceptual organization and the representation of natural form. In *Readings in Computer Vision*, pages 680–699. Elsevier, 1987. 3
- [44] Daxuan Ren, Jianmin Zheng, Jianfei Cai, Jiatong Li, Haiyong Jiang, Zhongang Cai, Junzhe Zhang, Liang Pan, Mingyuan Zhang, Haiyu Zhao, et al. Csg-stump: A learning friendly csg-like representation for interpretable shape parsing. In *Proceedings of the IEEE/CVF international conference on computer vision*, pages 12478–12487, 2021. 3
- [45] Sara Sabour, Suhani Vora, Daniel Duckworth, Ivan Krasin, David J. Fleet, and Andrea Tagliasacchi. Robustnerf: Ignoring distractors with robust losses. In *Proceedings of the IEEE/CVF Conference on Computer Vision and Pattern Recognition (CVPR)*, pages 20626–20636, 2023. 1, 2
- [46] Gopal Sharma, Rishabh Goyal, Difan Liu, Evangelos Kalogerakis, and Subhransu Maji. Csgnet: Neural shape parser for constructive solid geometry. In *Proceedings of the IEEE conference on computer vision and pattern recognition*, pages 5515–5523, 2018. 3
- [47] Tianchang Shen, Jacob Munkberg, Jon Hasselgren, Kangxue Yin, Zian Wang, Wenzheng Chen, Zan Gojcic, Sanja Fidler, Nicholas Sharp, and Jun Gao. Flexible isosurface extraction for gradient-based mesh optimization. *ACM Trans. Graph.*, 42(4), 2023. 2, 6, 7, 8
- [48] Yawar Siddiqui, Antonio Alliegro, Alexey Artemov, Tatiana Tommasi, Daniele Sirigatti, Vladislav Rosov, Angela Dai, and Matthias Nießner. Meshgpt: Generating triangle meshes with decoder-only transformers. *arXiv preprint arXiv:2311.15475*, 2023. 3
- [49] Robert W Sumner and Jovan Popović. Deformation transfer for triangle meshes. *ACM Transactions on graphics (TOG)*, 23(3):399–405, 2004. 2
- [50] Jia-Mu Sun, Tong Wu, and Lin Gao. Recent advances in implicit representation-based 3d shape generation. *Visual Intelligence*, 2(1):9, 2024. 2
- [51] Graham M Treece, Richard W Prager, and Andrew H Gee. Regularised marching tetrahedra: improved iso-surface extraction. *Computers & Graphics*, 23(4):583–598, 1999. 2, 6, 7

- [52] Shubham Tulsiani, Hao Su, Leonidas J Guibas, Alexei A Efros, and Jitendra Malik. Learning shape abstractions by assembling volumetric primitives. In *Proceedings of the IEEE Conference on Computer Vision and Pattern Recognition*, pages 2635–2643, 2017. [2](#)
- [53] Mikaela Angelina Uy, Vladimir G. Kim, Minhyuk Sung, Noam Aigerman, Siddhartha Chaudhuri, and Leonidas Guibas. Joint learning of 3d shape retrieval and deformation. In *IEEE Conference on Computer Vision and Pattern Recognition (CVPR)*, 2021. [3](#)
- [54] Peng Wang, Lingjie Liu, Yuan Liu, Christian Theobalt, Taku Komura, and Wenping Wang. Neus: Learning neural implicit surfaces by volume rendering for multi-view reconstruction. *NeurIPS*, 2021. [1](#), [2](#), [4](#)
- [55] Yiqun Wang, Ivan Skorokhodov, and Peter Wonka. Hf-neus: Improved surface reconstruction using high-frequency details. *arXiv preprint arXiv:2206.07850*, 2022. [2](#)
- [56] Yiming Wang, Qin Han, Marc Habermann, Kostas Daniilidis, Christian Theobalt, and Lingjie Liu. Neus2: Fast learning of neural implicit surfaces for multi-view reconstruction. In *Proceedings of the IEEE/CVF International Conference on Computer Vision (ICCV)*, 2023. [1](#)
- [57] Guanjun Wu, Taoran Yi, Jiemin Fang, Lingxi Xie, Xiaopeng Zhang, Wei Wei, Wenyu Liu, Qi Tian, and Xinggang Wang. 4d gaussian splatting for real-time dynamic scene rendering. In *Proceedings of the IEEE/CVF Conference on Computer Vision and Pattern Recognition (CVPR)*, pages 20310–20320, 2024. [2](#)
- [58] Yuwei Wu, Weixiao Liu, Sipu Ruan, and Gregory S. Chirikjian. Primitive-based shape abstraction via nonparametric bayesian inference. In *Computer Vision – ECCV 2022*, pages 479–495, Cham, 2022. Springer Nature Switzerland. [3](#)
- [59] Jiawei Yang, Marco Pavone, and Yue Wang. Freenerf: Improving few-shot neural rendering with free frequency regularization. In *Proc. IEEE Conf. on Computer Vision and Pattern Recognition (CVPR)*, 2023. [1](#), [2](#)
- [60] Lior Yariv, Yoni Kasten, Dror Moran, Meirav Galun, Matan Atzmon, Basri Ronen, and Yaron Lipman. Multiview neural surface reconstruction by disentangling geometry and appearance. *Advances in Neural Information Processing Systems*, 33:2492–2502, 2020. [1](#), [2](#)
- [61] Chongjie Ye, Lingteng Qiu, Xiaodong Gu, Qi Zuo, Yushuang Wu, Zilong Dong, Liefeng Bo, Yuliang Xiu, and Xiaoguang Han. Stablenormal: Reducing diffusion variance for stable and sharp normal. *ACM Transactions on Graphics*, 2024. [6](#)
- [62] Jingwen Ye, Yuze He, Yanning Zhou, Yiqin Zhu, Kaiwen Xiao, Yong-Jin Liu, Wei Yang, and Xiao Han. Primitiveanything: Human-crafted 3d primitive assembly generation with auto-regressive transformer. In *Proceedings of the IEEE/CVF Conference on Computer Vision and Pattern Recognition (CVPR)*, 2024. [3](#), [6](#), [7](#), [8](#)
- [63] Yuanyan Ye, Yubo Wang, Juan Cao, and Zhonggui Chen. Watertight surface reconstruction method for cad models based on optimal transport. *Computational Visual Media*, 10(5):859–872, 2024. [3](#)
- [64] Fenggen Yu, Zhiqin Chen, Manyi Li, Aditya Sanghi, Hooman Shayani, Ali Mahdavi-Amiri, and Hao Zhang. Capri-net: Learning compact cad shapes with adaptive primitive assembly. In *Proceedings of the IEEE/CVF conference on computer vision and pattern recognition*, pages 11768–11778, 2022. [3](#), [6](#), [7](#), [8](#)
- [65] Fenggen Yu, Qimin Chen, Maham Tanveer, Ali Mahdavi Amiri, and Hao Zhang. D2csg: Unsupervised learning of compact csg trees with dual complements and dropouts. *Advances in Neural Information Processing Systems*, 36: 22807–22819, 2023. [3](#), [6](#), [7](#), [8](#)
- [66] Zehao Yu, Anpei Chen, Binbin Huang, Torsten Sattler, and Andreas Geiger. Mip-splatting: Alias-free 3d gaussian splatting. In *Proceedings of the IEEE/CVF Conference on Computer Vision and Pattern Recognition (CVPR)*, pages 19447–19456, 2024. [2](#)
- [67] Haocheng Yuan, Adrien Bousseau, Hao Pan, Quancheng Zhang, Niloy J Mitra, and Changjian Li. Diffcsg: Differentiable csg via rasterization. In *SIGGRAPH Asia 2024 Conference Papers*, pages 1–10, 2024. [6](#), [7](#), [8](#)